Available online at www.sciencedirect.com

SciVerse ScienceDirect

Acta Materialia 59 (2011) 7368–7379

Acta MATERIALIA

www.elsevier.com/locate/actamat

Length-scale-dependent deformation and fracture behavior of Cu/X (X = Nb, Zr) multilayers: The constraining effects of the ductile phase on the brittle phase

J.Y. Zhang, X. Zhang, R.H. Wang, S.Y. Lei, P. Zhang, J.J. Niu, G. Liu *, G.J. Zhang, J. Sun *

State Key Laboratory for Mechanical Behavior of Materials, Xi'an Jiaotong University, Xi'an 710049, People's Republic of China

Received 5 July 2011; received in revised form 9 August 2011; accepted 12 August 2011
Available online 24 September 2011

Abstract

The plastic deformation and fracture behavior of two different types of Cu/X (X = Nb, Zr) nanostructured multilayered films (NMFs) were systematically investigated over wide ranges of modulation period (λ) and modulation ratio (η, the ratio of X layer thickness to Cu layer thickness). It was found that both the ductility and fracture mode of the NMFs were predominantly related to the constraining effect of ductile Cu layers on microcrack-initiating X layers, which showed a significant length-scale dependence on λ and η. Experimental observations and theoretical analyses also revealed a transition in strengthening mechanism, from single dislocation slip in confined layers to a load-bearing effect, when the Cu layer thickness was reduced to below ~15 nm by either decreasing λ or increasing η. This is due to the intense suppression of dislocation activities in the thin Cu layers, which causes a remarkable reduction in the deformability of the Cu layers. Concomitantly, the constraining effect of Cu layers on microcrack propagation is weakened, which can be used to explain the experimentally observed λ and η-dependent fracture mode transition from shear mode to an opening mode. Furthermore, the fracture toughness of the NMFs is also found to be sensitive to both λ and η. A fracture mechanism-based micromechanical model is developed to quantitatively assess the length-scale-dependent fracture toughness, and these calculations are in good agreement with experimental findings.

Keywords: Nanostructured multilayers; Deformability; Fracture behavior; Constraint effects; Length scale

1. Introduction

Nanostructured multilayered films (NMFs) are increasingly being considered for various applications because of improvements that have been made in the capability to tailor the fabrication of these structures to achieve specific properties. It is the large number of interfaces in the NMFs that determines the unique behavior of this special type of composite [1–6]. Under a constant modulation ratio (η) of 1, the hardness/strength curve of NMFs varies with individual layer thickness (one-half of the modulation period λ), and usually exhibits three different regions [7–11]: Hall–Petch (H–P) behavior in the first region, even greater dependence on the layer thickness in the second region, and a plateau or softening in hardness/strength in the third one. Correspondingly, three kinds of strengthening mechanism have been proposed to describe the variation in hardness/strength of these materials as their characteristic dimensions shrink toward to the nanoregime: (i) the H–P-like strengthening relationship based on dislocations piling up against the interface [1,7,12], which is applicable at the submicrometer to micron length scales; (ii) the confined layer slip (CLS) mechanism involving single dislocation loop glide confined to isolated layers [8,13,14], which works at length scales of a few to a few tens of nanometers; and

* Corresponding authors. Tel.: +86 (0)2982668695; fax: +86 (0)2982 663453.
E-mail addresses: lgsammer@mail.xjtu.edu.cn (G. Liu), junsun@mail.xjtu.edu.cn (J. Sun).

1359-6454/$36.00 © 2011 Acta Materialia Inc. Published by Elsevier Ltd. All rights reserved.
doi:10.1016/j.actamat.2011.08.016

(iii) the interface barrier strength (IBS) mechanism, which considers a single dislocation cutting cross the interface [15,16], and is operative at a length scale of a few nanometers.

In general, the strength and ductility of materials are mutually exclusive, i.e. the ductility of NMFs drops with decreasing λ, showing a reverse trend to the strength [17–21]. Huang and Spaepen [17] found that 3 μm thick free-standing Ag/Cu multilayers became increasingly stronger and less ductile with decreasing λ, and the Ag/Cu multilayers were macroscopically brittle when the λ was less than 80 nm. Other available experimental results on evaluating the strength and ductility of NMFs were recently reported by the Los Alamos Group [19–21]. By using nanoindentation testing, they compressed Cu/Nb NMMs pillars (4 μm in diameter) and found an increase in flow stress from 1.75 to 2.4 GPa when λ was reduced from 80 to 10 nm [19,20]. However, the ductility decreased from 36% to 25. Meanwhile, Misra et al.'s [22] results showed that the rolling strain to fracture of Cu/Nb multilayers decreased rapidly when the λ was less than about 60 nm. They attributed this to relative variations in yield strength and fracture stress, and subsequently proposed a dislocation mechanism transition from Orowan bowing to interface crossing [23]. Recently, Zhu et al. [24] suggested that the fracture mode of nanostructured Cu/Ta multilayers was directly related to the strengthening mechanism. They compared the damage behaviors of nanostructured Cu/Ta multilayers between $\lambda = 10$ and 250 nm, and found that the 10 nm multilayer exhibited shear-mode fracture while the 250 nm multilayer fractured in opening mode [24]. Based on theoretical analyses, they claimed that the shear-mode and opening-mode fracture was associated with strengthening via IBS and CLS, respectively [24].

All these above-mentioned experimental results further imply that the interface/boundary structure and the length scale of the constituent layers are the most important factors influencing the strength, ductility and fracture behavior of metallic multilayers. However, there have been few reports to quantitatively show the dependence of deformation and fracture behavior on the length scale (including λ and η) in NMFs. Thus, a careful examination of the deformation and fracture behavior of various multilayer systems at different length scales is helpful to better understand the toughening mechanism and to artificially control the properties of NMFs.

In this paper, two different types of NMFs, i.e. immiscible face-centered cubic (fcc)/body-centered cubic (bcc) Cu/Nb and fcc/hexagonal close-packed (hcp) Cu/Zr, were selected. The plastic deformation and fracture behavior of multilayers with λ ranging from 10 to 250 nm ($\eta = 1$) and of multilayers with η ranging from 0.11 to 3 ($\lambda = 25$ and 50 nm) were systematically investigated by means of uniaxial tensile tests. The effects of length scale and the constraining effects on the strength, ductility, fracture toughness and fracture mode of the Cu/X NMFs were examined experimentally and evaluated theoretically.

2. Experimental

Two kinds of Cu/X (X = Nb, Zr) NMFs were deposited on polyimide substrate by means of direct current magnetron sputtering at room temperature. The chamber was evacuated to a base pressure of $\sim 5 \times 10^{-8}$ Torr prior to sputtering, and pressures of 1.0–3 $\times 10^{-3}$ Torr Ar were used during deposition. In order to reveal the length-scale-dependent deformation clearly, the characteristic microstructural parameters of NMFs, λ and η (where η is the ratio of X layer thickness h_X to Cu layer thickness h_{Cu}, $\eta = h_X/h_{Cu}$), are changed independently. One series of NMFs has a constant modulation ratio η of 1, but a wide range of modulation period λ ($\lambda = h_X + h_{Cu}$) from 10 to 250 nm. The other series of NMFs has a constant λ ($\lambda = 25$ and 50 nm) but a wide range of η from 0.11 to 3.0. During deposition, the first layer on the polyimide substrate was X and the last layer was Cu. The total thickness of the multilayers was about 500 nm for Cu/Nb and about 1000 nm for Cu/Zr. The as-deposited Cu/X NMFs were annealed at 150 °C for 2 h to stabilize the microstructure and eliminate the residual stress. X-ray diffraction (XRD) was carried out using an improved Rigaku D/max-RB X-ray diffractometer with Cu K_α radiation and a graphite monochromator to determine the crystallographic texture and the residual stress by using "$\sin^2\psi$ method" [25]. High-resolution transmission electron microscopy (HRTEM) observations and energy-dispersive X-ray (EDX) analyses were performed to observe the modulation structure and the interface structure. For comparison, single-layer monolithic Nb and Zr films with thickness (h) falling within the 60–350 nm range were also prepared on polyimide substrate, following the same treatments as mentioned above.

Uniaxial tensile testing was performed by using a Micro-Force Test System (MTS® Tytron 250) at a constant strain rate of 1×10^{-4} s^{-1} at room temperature. All the samples have a total length of 65 mm, a gauge section of 30 mm in length and are 4 mm wide. The samples were strained to a given magnitude, i.e. ~10%. During tensile testing, the force and displacement were automatically recorded by machine; this can be subsequently converted into the stress–strain curves of the NMFs [26]. The yield strength ($\sigma_{0.2}$) is determined as the 0.2% offset. A macroscopic strain (ε_C) corresponding to a critical degree of microcracking (measured in situ using an electrical resistance change method [26]), instead of the rupture strain or elongation, is used to characterize the ductility. In order to analyze the failure mechanism, the Cu/X NMFs tested were cross-sectioned and characterized by dual-beam focused ion beam/scanning electron microscopy (FIB/SEM) using an FEI microscope. The fracture mode (e.g. opening and shear fracture) was characterized by the fracture angle θ, which is defined as the angle between the macrocracking direction and the horizontal direction.

3. Results

3.1. Microstructure

The high-angle symmetrical XRD spectra for Cu/X NMFs with constant η showed a strong $\langle 1\,1\,1\rangle$ out-of-plane texture in the Cu layers and a strong $\langle 1\,1\,0\rangle$ out-of-plane texture in the Nb layers (Fig. 1a), and $\langle 0\,0\,0\,2\rangle$ out-of-plane texture in the hcp Zr layers (Fig. 1c). The in-plane orientations are random in the constituent layers. The XRD spectra for Cu/X NMFs with constant λ revealed that, as η decreases, the diffraction peaks of X disappear, as shown in Fig. 1b and d. The residual stress was determined to be $\sim 200 \pm 100$ MPa for all the Cu/X NMFs with different λ and η, which is far lower than their yield strength (see below). Similarly, the residual stress in the single-layer Nb and Zr films was determined to be $\sim 180 \pm 80$ and 150 ± 50 MPa, respectively, and was also insensitive to film thickness.

Typical cross-sectional TEM images of some Cu/X NMFs with clear modulated layer structures are displayed in Fig. 2, where one can find columnar grains in the Cu layers and ultrafine nanocrystals in the X layers. The average grain sizes of both Cu and X layers scale with layer thickness. There is insignificant intermixing the Cu/Nb interfaces, as supported by the HRTEM image (Fig. 2b) and line-scanning analysis along the layer growth direction (Fig. 2c). The formation of insignificant intermixing between Cu and Nb layers is mainly related to the surface energy and the energetic non-equilibrium deposition process, similar to previous reports in binary immiscible metallic multilayers such as Cu/Ta [27], Ag/Nb [28] and Ag/Ni [29]. Fig. 2d is a representative cross-sectional view of Cu/Nb NMFs with $\eta = 0.2$ and $\lambda = 25$ nm. Because of the thinner dimension (~4 nm in thickness), the Nb layer is disordered to some extent and somewhat similar to amorphous phase (see Fig. 2e, inserted in Fig. 2d). This is probably the underlying reason why Nb diffraction peaks are not observed in the XRD patterns. The Cu/Zr NMFs behave the same way at small η. In addition, some incontinuous local amorphous regions 1–2 nm thick have been observed at the Cu/Zr interface (Fig. 2h). The diffusion of some Cu atoms into Zr layers is also revealed from the EDX analyses (not shown here).

3.2. Length-scale-dependent yield strength

3.2.1. Modulation-period-dependent yield strength

Fig. 3 shows a significant λ-dependence of $\sigma_{0.2}$ for the two Cu/X (X = Nb, Zr) NMFs at constant $\eta = 1$. Within the λ range from 250 nm down to about 25 nm, $\sigma_{0.2}$ gradually increases with reducing λ, in broad agreement with general observations that smaller is stronger. No further apparent increase in $\sigma_{0.2}$ will be found when λ is less than 25 nm. This means $\sigma_{0.2}$ reaches a saturation value at this size regime. For comparison, the strength of 60 nm thick single-layer nanocrystalline Cu, Nb and Zr films experimentally determined in present work are also plotted in Fig. 3.

3.2.2. Modulation-ratio-dependent yield strength

Fig. 4 shows that $\sigma_{0.2}$ of the two Cu/X NMFs is also sensitive to η. $\sigma_{0.2}$ increases remarkably with increasing η up to ~1.0, beyond which $\sigma_{0.2}$ increases slowly. The behavior of the η-dependent $\sigma_{0.2}$ is somewhat complicated as it is coupled with the effect of λ. Within the region of η lower than

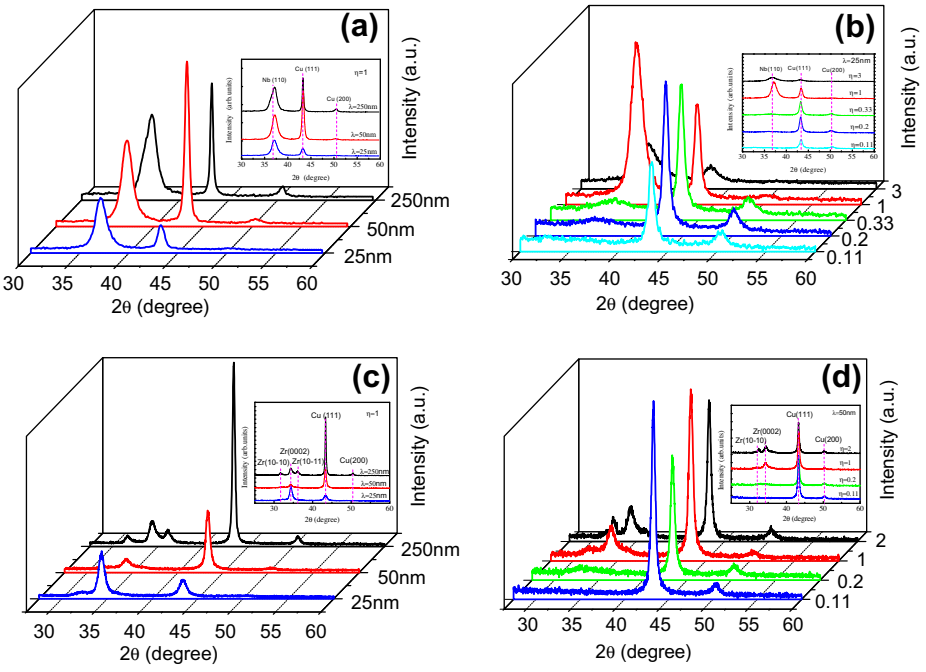

Fig. 1. XRD spectra of Cu/Nb ((a) $\eta = 1.0$ and (b) $\lambda = 50$ nm) and Cu/Zr ((c) $\eta = 1.0$ and (d) $\lambda = 50$ nm) NMFs.

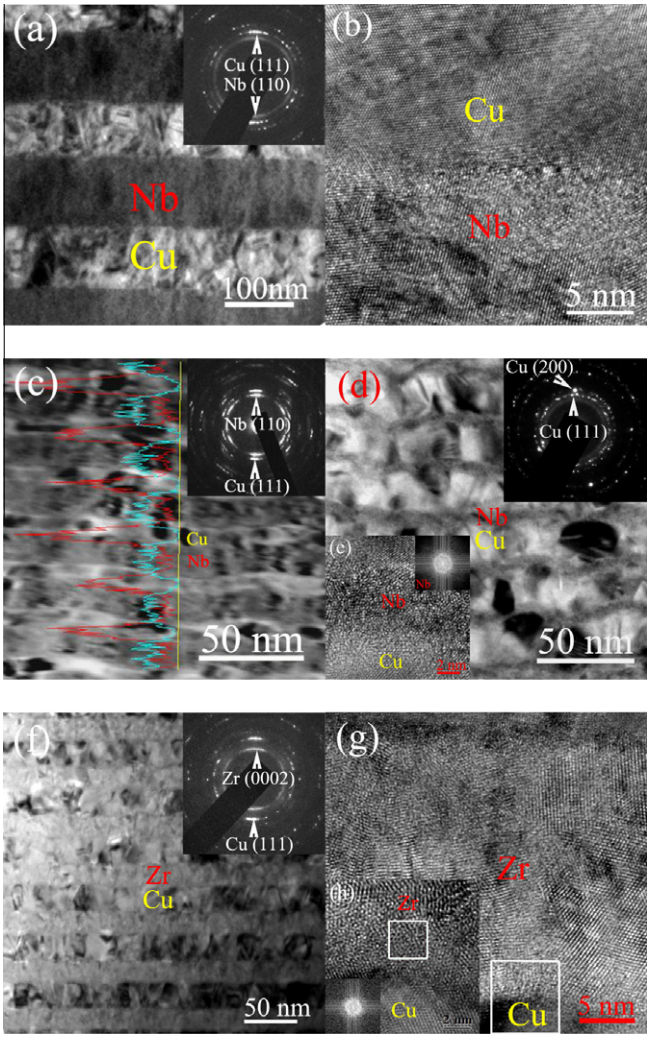

Fig. 2. Bright-field cross-sectional TEM micrograph showing the microstructure of the $\eta = 1.0$ Cu/Nb NMFs with (a) $\lambda = 125$ nm and (c) $\lambda = 25$ nm, (d) $\eta = 0.2$ Cu/Nb NMFs with $\lambda = 25$ nm, and (f) $\eta = 1.0$ Cu/Zr NMFs with $\lambda = 50$ nm. Insert is the corresponding selected-area diffraction pattern. Line scanning analysis in (c) shows the chemical modulation structure. (b, e and g) are HRTEM images showing the Cu/X interface, and (h) is the magnification of the square boxed region in (g). Insets in (e and h) are the Fourier transform of the Nb layer and of the square boxed area in the Zr layer, respectively.

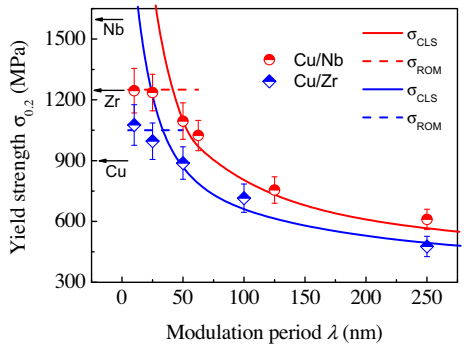

Fig. 3. Dependence of $\sigma_{0.2}$ on λ for the Cu/X NMFs with $\eta = 1.0$. Solid curves are calculations from CLS model and the dashed curve is from the rule-of-mixtures (ROM). The strength of 60 nm thick-single layer Cu, Nb and Zr films are also plotted, as indicated by arrows.

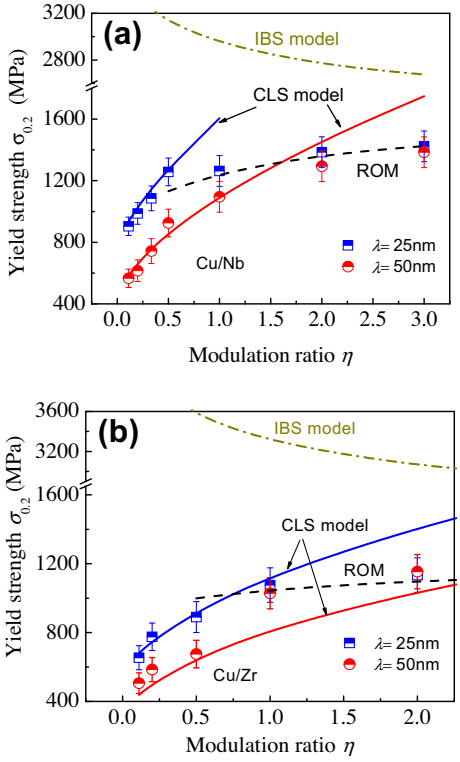

Fig. 4. Dependence of $\sigma_{0.2}$ on η for (a) the Cu/Nb and (b) the Cu/Zr NMFs with $\lambda = 25$ and 50 nm, respectively. Solid curves are calculations from CLS model, dash-dotted curve is from IBS model and dashed curve is from the rule-of-mixtures (ROM).

1.0 (or $h_{Cu} > 15$ nm), the $\lambda = 25$ nm NMFs exhibit $\sigma_{0.2}$ obviously larger than those with $\lambda = 50$ nm. When η is above 1.0 (or $h_{Cu} < 15$ nm), however, the NMFs with different modulation periods of 25 and 50 nm have almost the same yield strength.

3.3. Length-scale-dependent ductility

3.3.1. Modulation-period-dependent ductility

Fig. 5a shows the dependence of ε_C on h_{Cu} for Cu/X NMFs with constant $\eta = 1$, and of ε_C on h for single-layer Nb and Zr films. Similar to what was observed in single-layer Cu films [26], the Nb and Zr films exhibit a monotonic decrease in ε_C with reducing h. However, the Nb and Zr films have far lower ε_C than the Cu films. For example, the ductility (ε_C) of 340 nm thick Cu film is about 9% [26], while that of 350 nm thick Nb film is only about 0.85%. We thus simply refer hereafter to Nb (and Zr) as the brittle layer and to Cu as the ductile layer. Interestingly, as shown by Fig. 5a, over this h_{Cu} range the ε_C of the NMFs increases first, followed by a peak at a critical $h_{Cu}^{cri} \sim 25$ nm (or $\lambda^{cri} \sim 50$ nm). Below h_{Cu}^{cri}, ε_C decreases with reducing h_{Cu}, similar to the behavior of single-layer films, while above h_{Cu}^{cri}, a smaller h_{Cu} leads to higher ε_C. The unusual size-dependent ductility observed here indicates that the failure mechanisms for the Cu/X NMFs studied here are complicated and the controlling mechanisms are different within the two regions below and above

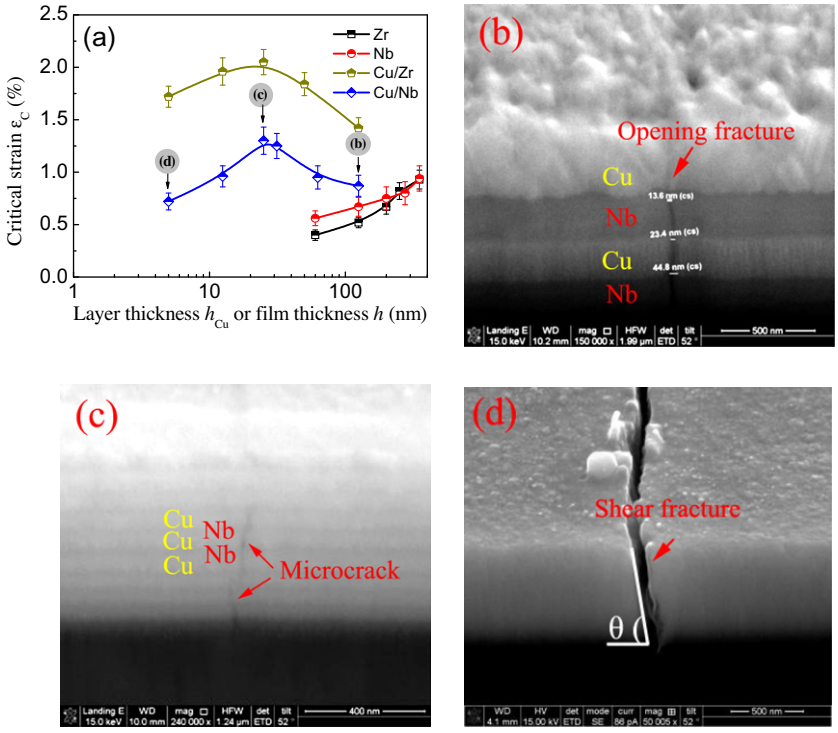

Fig. 5. (a) Dependence of ε_C on h_{Cu} for the Cu/X NMFs with $\eta = 1.0$ and on h for the single-layer Nb and Zr films. Lines are visual guides. Cu/Nb NMFs after testing with (b) $h_{Cu} = 125$ nm, (c) $h_{Cu} = 25$ nm, and (d) $h_{Cu} = 5$ nm are displayed in the corresponding panels, respectively, with FIB cross-sectional images of microcracks.

h_{Cu}^{cri}; it also suggests that the ductility of Cu/X NMFs can be maximized by tailoring their microstructure.

Microstructural observations were carried out to analyze the failure mechanisms of the Cu/X NMFs. Fig. 5b–d show typical FIB cross-sectional images of the tested samples with $\lambda = 250$, 50 and 10 nm, respectively (here only Cu/Nb NMFs are shown; Cu/Zr NMFs behave the same way). Microcracks are seen to initiate within and run across the Nb layer, which is the more brittle of the two constituent materials. As the λ decreases, the fracture angle θ monotonically decreases as well.

3.3.2. Modulation-ratio-dependent ductility

In contrast to the monotonic increase of $\sigma_{0.2}$, the ductility ε_C of Cu/X NMFs reduces monotonically with increasing η (Fig. 6). This indicates that an increase in the fraction of Cu results in the improved ductility of Cu/X NMFs. The striking feature is that, as η reduces down to below a critical η^{cri} (~0.5 for Cu/Nb, ~1.0 for Cu/Zr), the ductility of $\lambda = 25$ nm Cu/X NMFs is higher than that of $\lambda = 50$ nm NMFs at a given η; above η^{cri}, the larger λ is, the higher ε_C. This means that the Cu/X NMFs with small η (below η^{cri}) and λ can exhibit high ductility and high strength in combination, which is significant for engineering applications.

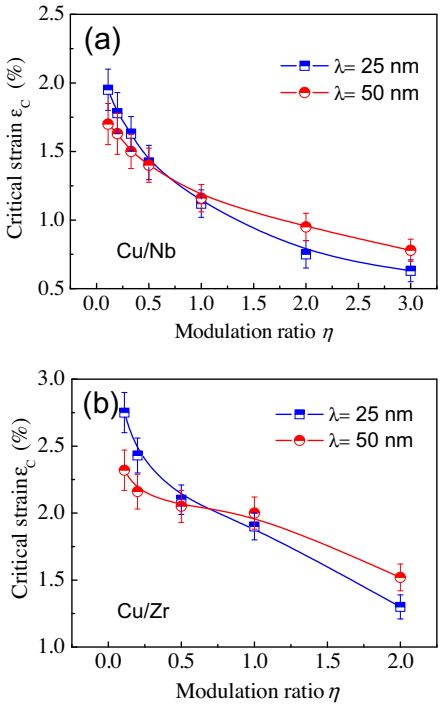

Fig. 6. Dependence of ε_C on η for (a) the Cu/Nb and (b) the Cu/Zr NMFs with $\lambda = 25$ and 50 nm, respectively.

3.4. Length-scale-dependent fracture mode

3.4.1. Modulation-period-dependent fracture mode

FIB cross-sectional observations (Fig. 5b–d) show that, within the λ range from 250 nm to about 60 nm, the Cu/X NMFs exhibit brittle opening fracture with $\theta \approx 83 \pm 3°$, as typically shown in Fig. 5b for the case of $\lambda = 250$ nm. By further reducing λ, the Cu/X NMFs tend to fracture in a shear mode and the fracture angle gradually decreases down to

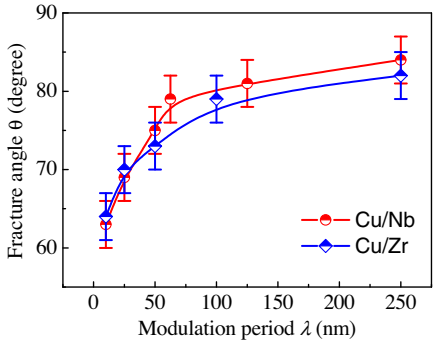

Fig. 7. Dependence of θ on λ for the Cu/X NMFs with $\eta = 1$.

about 65°. The images in Fig. 5c with $\theta \approx 75 \pm 3°$ for $\lambda = 50$ nm and in Fig. 5d with $\theta \approx 65 \pm 3°$ for $\lambda = 10$ nm clearly demonstrate the evolution in fracture mode from that shown in Fig. 5b. The conclusion drawn here that the Cu/X NMFs with smaller λ are more apt to fracture in a shear mode (Fig. 7) agrees well with previous observations in Cu/Nb nanolaminates tested by compression [19,20] and room-temperature rolling [23].

3.4.2. Modulation-ratio-dependent fracture mode

Fig. 8a and b shows the experimentally determined θ as a function of η for the two Cu/X NMFs under different λ of 25 and 50 nm, respectively. Within the wide η range from 3 down to 0.11, both these NMFs exhibit a monotonic reduction of θ from $\sim 84 \pm 3°$ to $\sim 52 \pm 4°$, indicating a fracture mode transition from brittle opening (Fig. 8c) to ductile shear (Fig. 8d). In other words, higher ε_C corresponds to smaller θ. Interestingly, the critical η for the opening-mode to shear-mode transition is almost the same ($\eta^{cri} \sim 1$) for the two types of NMFs, and all the NMFs have similar θ at the same η, regardless of the difference in λ (25 and 50 nm) and constituent phases (Cu/Nb and Cu/Zr).

4. Discussion

4.1. Scaling behavior of yield strength

The deformation and fracture behavior in NMFs is distinct from those in single-layer films owing to the presence of interfaces. The high strength of Cu/X NMFs (Figs. 3 and 4) can be ascribed to the constraining of dislocation activities due to the abundance of heterogeneous interface. The change in variation of $\sigma_{0.2}$ can be attributed to the transition in strengthening mechanism. With regard to the metallic multilayers composed of a softer/ductile layer and a harder/brittle layer, flow is controlled by the softer/ductile phase and thus the strengthening is closely linked to the smaller microstructural dimension between the layer thickness and grain size [15,16]. In the present Cu/X NMFs, the thickness of the Cu layers is much finer than the grain size, and hence h_{Cu} is the characteristic dimension controlling the flow behavior of the NMFs.

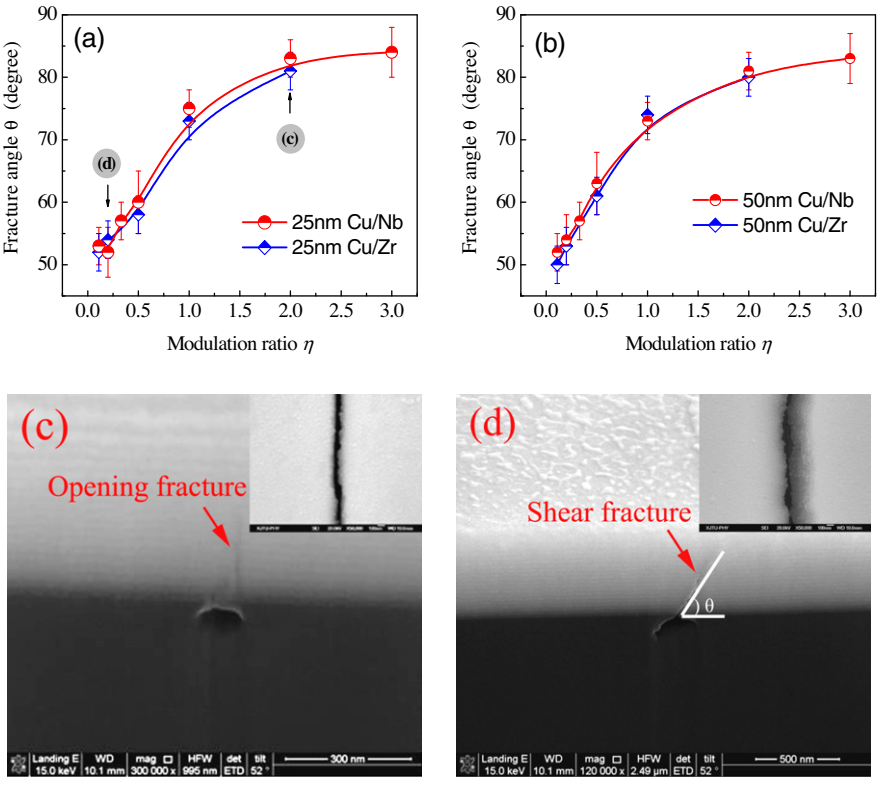

Fig. 8. Dependence of θ on η for the Cu/X NMFs with (a) $\lambda = 25$ nm and (b) $\lambda = 50$ nm, respectively. Curves are visual guides. The FIB cross-sectional images of (c and d) showing shear mode and opening mode, in $\lambda = 25$ nm Cu/X NMFs with $\eta = 2.0$ and $\eta = 0.2$, respectively. Insets show the corresponding SEM plan-view image of the NMFs, which can be used to further demonstrate the shear and opening fracture modes.

The CLS model [8,13,14] and IBS model will be used here for quantitative calculations, because the two models consider the modulus mismatch between constituent layers [15] as well as the misfit dislocations/interface interaction [16] at the nanoscale. When the CLS stress (σ_{CLS}) to drive the dislocation glide exceeds the IBS stress (σ_{IBS}) to drive the dislocation across the interface, the strengthening mechanism will transition from CLS to IBS, the strength of metallic multilayer will reach a saturation and no further apparent increase in strength will be observed as the layer thickness further decreases.

According to the CLS model, the applied stress σ_{CLS} required to propagate a glide dislocation loop confined to one Cu layer is given by [8]:

$$\sigma_{CLS} = M\frac{\mu^* b}{8\pi h'}\left(\frac{4-\nu}{1-\nu}\right)\ln\frac{\alpha h'}{b} + \frac{f}{h} + \frac{\mu^* b}{L(1-\nu)}, \quad (1)$$

where M is the Taylor factor; $h' = h_{Cu}/\sin\varphi$ is the layer thickness parallel to the glide plane; φ is the angle between the slip plane and the interface; b is the absolute length of the Burgers vector; ν is the Poisson ratio of Cu; $\mu^* = \frac{\mu_X \cdot \mu_{Cu}}{2(V_X \cdot \mu_{Cu} + V_{Cu} \cdot \mu_X)}$ is the mean shear modulus of Cu/X multilayer which can be estimated by the shear modulus μ_{Cu} and volume fraction V_{Cu} of the Cu layer and those of the X layer; α represents the core cut-off parameter; f is the characteristic interface stress of multiplayer; L is the mean spacing of glide loops in a parallel array ($L = bm/\varepsilon V_x$ [13]); V_x is the volume fraction of the X layer that is directly related to the η (i.e. $V_x = \eta/(1+\eta)$); ε is the in-plane plastic strain; and m is a strain resolution factor of the order of 0.45 for the active slip systems. Tensile data on nanoscale metallic multilayers [3,5,17] showed a low work-hardening rate after the initial 1–2% plastic strain. Misra et al. [8] also found that, using the CLS mode, a multilayer flow stress corresponding to a plastic strain of around 1–2% correlated well with the hardness measurement. Following this treatment, ε is chosen as 1% here to calculate the yield strength of Cu/X NMFs by using Eq. (1). With the parameters $M = 3.06$, $\mu_{Cu} = 48.3$ GPa, $\mu_{Nb} = 37.5$ GPa, $\mu_{Zr} = 33$ GPa, $\nu = 0.343$, $b = 0.2556$ nm, $\alpha = 0.2$ (for Cu/Zr) and 1 (for Cu/Nb), $f = 2 - 3$ J m^{-2} and $\varphi = 70.5°$, the dependence of σ_{CLS} on λ and η is quantitatively calculated and shown in Figs. 3 and 4 as the solid curves. The calculations fit well with the tensile yield strength data in the gradually increasing region (i.e. λ above 25 nm for $\eta = 1$ (see Fig. 3), η below 0.5 for $\lambda = 25$ nm and below 1.0 for $\lambda = 50$ nm (see Fig. 4)). Further decreasing λ (Fig. 3) or increasing η (Fig. 4), results in the CLS model being no longer applicable as it overestimates the yield strength too much. This suggests that another strengthening mechanism must be operating. The most likely mechanism seems to be IBS, i.e. single dislocations cutting across the interface instead of slipping in the confined layer [8].

The IBS is characteristic of interfacial structure and strongly influenced by lattice mismatch and shear modulus mismatch between two constituent layers [8,15,16]. Hence, if the interfacial structure does not change with λ, the σ_{IBS} should remain independent of the λ, which is given by [15,16]:

$$\sigma_{IBS} = M\beta\mu^*\left(\zeta - \frac{b}{L}\right) + \frac{MR\mu_{Cu/X}\sin\varphi}{8\pi}, \quad (2)$$

where β is Saada's constant; $R = |\mu_X - \mu_{Cu}|/|\mu_X + \mu_{Cu}|$; $\mu_{Cu/X}$ is the modulus of rigidity of the low-elastic-constant constituent for the Cu/X NMFs; ζ is the lattice mismatch between the constituent layers; L is a parallel array of glide loops of spacing; and the other symbols have the same as meaning defined previously. One can find that σ_{IBS} is a function of η (or μ^*). Substituting $\varphi = 70.5°$, $\beta \approx 0.4$, $\zeta = 10.5\%$ (for Cu/Nb) and $\zeta = 11.2\%$ (for Cu/Zr) into Eq. (2), the calculated σ_{IBS} are also found to be much higher than the experimental values (for $\eta = 1$ Cu/Nb and Cu/Zr, the σ_{IBS} are 2.94 and 3.14 GPa, respectively, not shown in Fig. 3). Again, the IBS model cannot explain the experimental strength results of the present Cu/X NMFs at small length scales, and another mechanism needs to be invoked.

In fact, at small length scales ($h_{Cu} < 15$ nm), the nucleation of dislocations from the dislocation sources is very difficult because larger nucleation stress is needed [30–32] and the pre-existing dislocations in the very thin Cu layers (thinner than ~15 nm) are strongly pinned by the interfaces. This sharply reduces the tensile deformability of the Cu/X NMFs and causes embrittlement of the materials (characterized by low ductility, as mentioned above). Consequently, the NMFs can be regarded as a kind of composite consisting of two hard/brittle layers, with the following (approximate) features: (i) both the two constituent layers behave as perfectly linear elastic materials and no interaction occurs between the constituent layers during straining; (ii) the interface bonding between the two constituent layers is perfect; (iii) no large defects such as voids are present; (iv) both the constituent layers are continuous and distributed uniformly (i.e. modulation structure). Under these conditions, the strength of NMFs can be simply described by the rule-of-mixtures (ROM) or the volume-weighted sum of the strength of the constituents. Because the yield strength is very close to the tensile strength in brittle materials, such as the constrained NMFs with ultrathin modulation structure, the yield strength is given as:

$$\sigma_{ROM} = V_{Cu}\sigma^*_{Cu} + V_X\sigma^*_X = \sigma^*_X - \frac{(\sigma^*_X - \sigma^*_{Cu})}{(1+\eta)}, \quad (3)$$

where σ^*_{Cu} and σ^*_X are the tensile yield strength of strongly constrained Cu layers and X layers. Based on tensile test on the 60 nm thick single-layer Cu, Nb and Zr films, the parameters for calculations are estimated as $\sigma^*_{Cu} =$ 900 MPa [25], $\sigma^*_{Nb} = 1600$ MPa and $\sigma^*_{Zr} = 1250$ MPa. The values of σ^*_{Cu}, σ^*_{Nb} and σ^*_{Zr} used here are close to previously reported values (estimated from 1/3 of hardness) of ~953 MPa for Cu [33], ~1860 MPa for Nb [33] and

~1350 MPa for Zr [34]. By using these values, Eq. (3) yields results that fit well with experimental values falling outside the CLS model—see the dashed curves in Figs. 3 and 4. Experimental results combined with theoretical analyses thus indicate that if h_{Cu} is reduced down to about 15 nm, the strengthening mechanism in the Cu/X NMFs transitions from the slide of single dislocations confined to individual Cu layers to the load-bearing effect that is similar that found in some composites.

4.2. Singularity of ductility

According to FIB observations (Figs. 5b–d, 8c, and d), the microcracks initiate within, and subsequently run across, the X layers, because the X layers with lower deformation capability (Fig. 5a) have more difficulty in accommodating the strain. Further propagation of the microcracks will be arrested by the more ductile Cu layers (Fig. 5b and c). Whether the microcracks can be stopped depends on two factors. The first is the intensity of stress–strain fields (ISF) ahead of the microcrack tip. ISF scales with $\sqrt{h_X}$ [35] as the size of the crack is approximately h_X. This would lead to the expectation that a smaller h_X is favorable for suppressing crack growth and improving ductility. The other factor is the shielding of microcrack propagation by the plastic deformation in Cu, which become rather limited when h_{Cu} is too small. This renders very thin Cu less effective in improving ductility. The two competing effects lead to the peak in the λ dependence and the maximum in ductility observed in Fig. 5a.

In the Cu/X NMFs with constant $\eta = 1$ and h_{Cu} above h_{Cu}^{cri}, plastic deformation in the Cu layers is not a problem and the ISF is the controlling factor. Reducing h_{Cu} would then promote crack suppression and improve ε_C. Indeed, comparing Fig. 5b and c, shorter and multiple isolated cracks are observed in thinner Nb layers. Only at $h_{Cu} = 125$ nm can the microcrack in the Nb layer overcome the Cu shielding effect and penetrate across the entire NMF. Below h_{Cu}^{cri}, the very thin Cu layers themselves become increasingly brittle as they lose the ability to accommodate dislocation activities, weakening the shielding effect of the Cu layers. The microcracks in the Nb layers, although small, can now break loose and cause failure (Fig. 5d). As a result, the NMF ductility shows an opposite trend and decreases with h_{Cu} (Fig. 5a).

In the case of Cu/X NMFs with constant λ, some dislocations in the Cu layers are movable and the Cu layers have some deformability which can shield the propagation of tiny microcracks in the CLS-applicable region (i.e. below η^{cri}). The thinner the h_X or microcrack size, the more possible it is for the Cu layers to arrest the microcracks. The Cu/X NMFs with $\lambda = 25$ nm have h_X only half of that in $\lambda = 50$ nm, and therefore show a higher ductility. Beyond the CLS-applicable region (i.e. above η^{cri}), the NMFs appear to be equivalent to composites consisting of alternate brittle Cu layers and brittle X layers, in which the higher number of weak interfaces will remarkably degrade the deformability in $\lambda = 25$ nm, causing the ductility to be lower than that in $\lambda = 50$ nm.

4.3. Transition of opening-mode to shear-mode fracture

From Fig. 5b–d, we can draw the conclusion that the NMFs with $\eta = 1$ will fracture in a shear mode only when λ approaches the nanometer scale (also see Fig. 7). According to Zhu et al.'s suggestions [24], the change from opening-mode to shear-mode fracture in the present Cu/X NMFs at critical $\lambda^{cri} \approx 60$ nm may be related to the change in strengthening mechanism from CLS to IBS. In the IBS-applicable regions, the dislocation would transmit across the interface to cause a shear offset, finally resulting in shear-mode fracture. In the CLS regions, however, the dislocation glide is confined to one layer and no dislocation will transmit across the interface; the increasing local stress concentration ahead of the crack will then cause an opening-mode fracture [24]. In brief, the λ-dependent fracture mode of NMFs was previously explained by the length-scale dependence of the transition of the strengthening mechanism from CLS to IBS.

In the present Cu/X NMFs with constant λ, we further find that the fracture mode of NMFs is also η-dependent. The transition from opening-mode to shear-mode fracture is observed at $\eta^{cri} \approx 1.0$. For quantitative reasons, calculations are performed again by using Eqs. (1) and (2) to see whether the η-dependent change in fracture mode is also a result of the transition from CLS to IBS strengthening. The calculation results are shown in Fig. 4. It can be seen that both σ_{IBS} and σ_{CLS} depend remarkably on η. However, the theoretical transition point, or the intersection point η^{cri} between the σ_{IBS} and σ_{CLS} curves, is much larger than the experimental results of $\eta^{cri} \approx 1.0$. For example, the predicted η^{cri} is ~7.0 and ~3.5 for Cu/Nb (~20.0 and ~11.0 for Cu/Zr) at $\lambda = 50$ and 25 nm, respectively. From the extensive experimental results shown here, we can conclude that the dominant factor controlling the fracture mode transition in NMFs is in fact not the transition of the strengthening mechanism from CLS to IBS. Moreover, analyses of the strengthening mechanisms discussed above also revealed that it is the ROM rather than the IBS model that operates at small λ and/or large η. In the following, a constraining effect of the ductile layer on the brittle layer is proposed to be the dominant factor controlling the ductility and the opening-to-shear transition in fracture mode, and is quantitatively assessed by using a micromechanical model.

As mentioned above, further propagation of the microcracks is arrested by the more ductile Cu layers (Fig. 5b and c). Whether the microcracks can be stopped depends on two factors. One is the ISF ahead of the microcrack tip, scaling with $\sqrt{h_X}$ [35] as the crack size is approximately h_X. One can then expect that a smaller h_X is favorable for suppressing microcrack growth and yielding shear-mode fracture. This is the case in Fig. 7 with $\eta = 1$, where the decrease in λ means a reduction in h_X and so shear-mode

fracture can be observed at smaller λ. The other factor is the shielding of microcrack propagation by the dislocation activities in Cu, which become rather limited when h_{Cu} is too small. In other words, very thin Cu is less effective in hindering opening fracture. This is the case at larger η (Fig. 8a and b), where the Cu layer is much thinner compared with the X layer and so the NMFs fracture in opening mode.

The propagation of microcracks can be analyzed in the framework of fracture mechanics. A micromechanical fracture model [36] is subsequently employed to describe the constraining effect on microcrack propagation. This model was selected in order to consider the effect of dislocation confinement on fracture behavior in laminates consisting of alternating ductile and brittle layers. Because the ductile layers have a size far below the micron level, dislocations must be treated individually. As discussed above, microcracks are initiated in the brittle X layers and are blocked by the interface, as schematically shown in Fig. 9a. Dislocations emitted from the microcrack tip have two effects: (i) they blunt the crack-tip and thereby reduce the tensile stress at the crack tip; and (ii) they pile up against an interface and send a back-stress to the crack tip that hinders further dislocation emission. At a given load level, an equilibrium number (n) of dislocations exists, which can be given as [36]:

$$n = \frac{4\pi(1-\nu)}{\ln(\bar{h}/\bar{r})}\left(\frac{\overline{K}_{app}\sqrt{\bar{h}}}{A\sqrt{2\pi}}\sin\phi\cos\frac{\phi}{2} - \bar{\gamma}\right), \tag{4}$$

where φ is the angle that the slip plane inclines from the interface (chosen as 45° without loss of generality); A is a factor slightly greater that unity; $\bar{r} \approx 2.7r_0/b$ with r_0 being the effective core radius of dislocation ($r_0 = 1.725$ nm) and b the Burgers vector of the ductile Cu ($b = 0.256$ nm); $\overline{K}_{app}$, $\bar{h}$ and $\bar{\gamma}$ are normalized values of the far-field mode I stress intensity K_{app}, the maximum distance $h_\varphi = h_{Cu}/\sin\varphi$ that the leading dislocation can travel, and the surface energy γ, respectively:

$$\overline{K}_{app} = \frac{K_{app}}{\mu\sqrt{b}}, \quad \bar{h} = \frac{h_\phi}{b}, \quad \bar{\gamma} = \frac{\gamma}{\mu b}, \tag{5}$$

where μ is the shear modulus of the Cu layers. The tensile stress at the blunted crack tip ($\bar{\sigma}_{tip} = \sigma_{tip}/\mu$) is related to n and $\overline{K}_{app}$ as [36]:

$$\bar{\sigma}_{tip}\sqrt{n} = 2\sqrt{\frac{2}{\pi}}\overline{K}_{app}\left(1 - \frac{3\left(\sin\phi\cos\frac{\phi}{2}\right)^2}{\ln(\bar{h}/\bar{r})}\right) + \frac{12A}{\sqrt{\bar{h}}\ln(\bar{h}/\bar{r})}\bar{\gamma}\sin\phi\cos\frac{\phi}{2}. \tag{6}$$

If the applied load is increased, competition between further dislocation emission and cleavage at the blunted crack tip will take place. When the microcrack tip tensile stress $\bar{\sigma}_{tip}$ reaches the normalized cohesive strength of the material, $\bar{\sigma}_c$ ($=\sigma_c/\mu$), fracture (cleavage) occurs in the ductile Cu layer and the pre-existing microcrack will propagate to form an opening fracture. Based on this criterion, the maximum number of dislocations emitted from the microcrack tip prior to cleavage (n_{max}) and the far-field I stress intensity ($\overline{K}_{app}$) or $\overline{K}_{IC}$ can be resolved from Eqs. (4) and (6) in combination. The crack tip stress intensity ($\overline{K}_{tip}$) is finally obtained as [36]:

$$\overline{K}_{tip} = \overline{K}_{app} - \frac{An}{(1-\nu)\sqrt{2\pi b\bar{h}}}\frac{3}{2}\sin\phi\cos\phi. \tag{7}$$

Calculations are performed and the results for $\overline{K}_{tip}$ vs. λ and $\overline{K}_{tip}$ vs. η are respectively obtained at a reasonable value $\bar{\sigma}_c = 0.2 - 0.4$ that is applicable to ductile metals such as Cu [36]. The predicted results (for $\bar{\sigma}_c = 0.4$) are shown in Fig. 9b and c, respectively. In the $\overline{K}_{tip}$ vs. λ curves, the crack tip stress intensity notably reduces below $\lambda \approx 60$–80 nm at $\eta = 1$. Similarly in the $\overline{K}_{tip}$ vs. η curves, $\overline{K}_{tip}$ sharply decreases below $\eta \approx 0.8$–0.9 over a wide range of λ from 25 to 100 nm. As is well known, a larger ISF indicates that the microcrack can propagate more easily to form an opening fracture. The predictions from Fig. 9b and c reveal that the transition in fracture mode, from opening to shear,

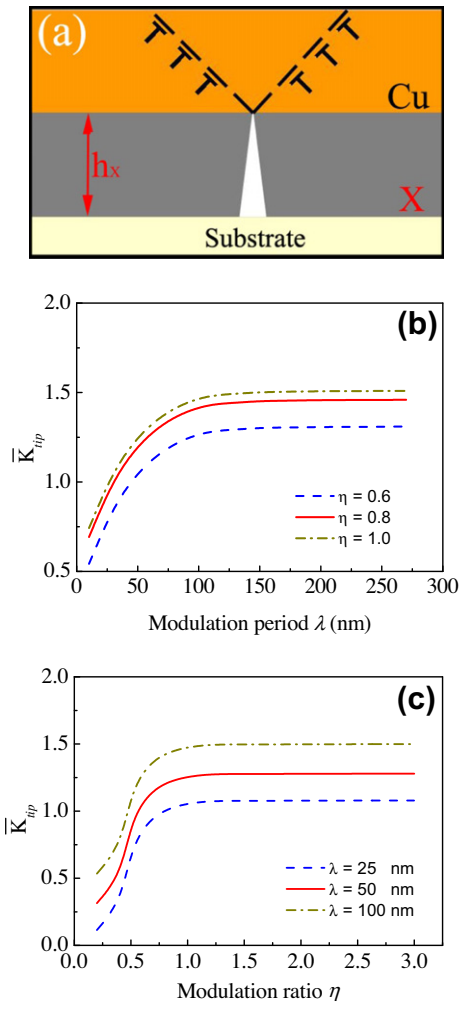

Fig. 9. (a) Sketch of the micromechanical fracture model. (b) Dependence of $\overline{K}_{tip}$ on η as a function of λ. (c) Dependence of $\overline{K}_{tip}$ on λ as a function of η.

may occur at the critical condition of $\lambda^{cri} \approx 60$–80 nm ($\eta \approx 1$) or $\eta^{cri} \approx 0.8$–0.9 (λ from 25 to 100 nm), which is in broad agreement with the present experimental results.

4.4. Length-scale-dependent toughness

The utility of nanostructured multilayers in engineering applications depends ultimately on their strength and toughness. The fracture toughness K_{IC} can be calculated by linear elastic fracture mechanics [37]. The cracking of brittle films on polyimide substrate is described analytically by 2-D steady-state models [37], in which the crack driving force, i.e. the steady-state energy release rate ξ, only depends on the shape of the crack tip, which is maintained as the crack propagates. Thus ξ is independent of the crack size, which can be expressed as [37]:

$$\xi = \frac{\pi\sigma^2 h_T}{2E}(1-\nu^2)g(\alpha,\beta), \tag{8}$$

where E is the Young's modulus of the NMFs; ν is the Poisson's ratio ($\sim$1/3); σ is the tensile stress of NMFs at ε_C, which can be determined from th stress–strain curve of the films; h_T is the total multilayer thickness; and $g(\alpha, \beta)$ is a dimensionless quantity that can be calculated from the elastic mismatch between the film and substrate, with α and β being the two Dundurs' parameters [38] characterizing the elastic mismatch between film and substrate. For a brittle and stiff film on a compliant substrate the value of $g(\alpha, \beta)$ is about 1.3–24, whereas, for our case of Cu/X multilayers on polyimide, $g(\alpha, \beta)$ is estimated (through interpolation) according to Ref. [37]. Thus, the fracture toughness (K_{IC}) of the Cu/X NMFs is generally given by [1]:

$$K_{IC} = \sqrt{\frac{E\xi}{1-\nu^2}}. \tag{9}$$

For the present NMFs, $\alpha \cong 0.93$ for Cu/Nb, $\alpha \cong 0.92$ for Cu/Zr and $\beta = \alpha/4$. Using experimental data together with Eqs. (8) and (9), K_{IC} is calculated as a function of h_{Cu}, as shown in Fig. 10a. The λ-dependent K_{IC} behaves similarly to ε_C, and also has a maximum at $h_{Cu} = 25$ nm.

The K_{IC} behavior in fact fits well with the predictions from the micromechanical fracture model [36] mentioned above. According to Hsia et al. [36], the fracture mode of the confined layered metals could be cleavage because the dislocation activities are intensely limited. When the microcrack tip tensile stress $\bar{\sigma}_{tip}$ reaches the normalized cohesive strength of the material, the far-field applied stress intensity under this condition is then the fracture toughness of the layered films, i.e. $\overline{K}_{IC} = \overline{K}_{app}|_{\bar{\sigma}_{tip}=\bar{\sigma}_c}$, which can be obtained from Eqs. (4) and (6). Calculations of $\overline{K}_{IC}$ vs. h_{Cu} (shown in Fig. 10a) also reveal a maximum value at $h_{Cu}^{cri} \approx 25$ nm. In particular, the calculations at $\bar{\sigma}_c = 0.3$–0.4 fit well with the measurements.

The predictions for n_{max}, Fig. 10b, support our explanation of the length-scale-dependent ductility and toughness. It can be seen that n_{max} sharply decreases when h_{Cu} is reduced down to less than about h_{Cu}^{cri}, quantitatively demonstrating that the Cu layer will lose much of its plastic deformation capability and thus become more brittle because few dislocations can be emitted. Conversely, with appropriate selection of h_{Cu} at or slightly above h_{Cu}^{cri}, high ductility can be achieved in the NMFs with enhanced strength.

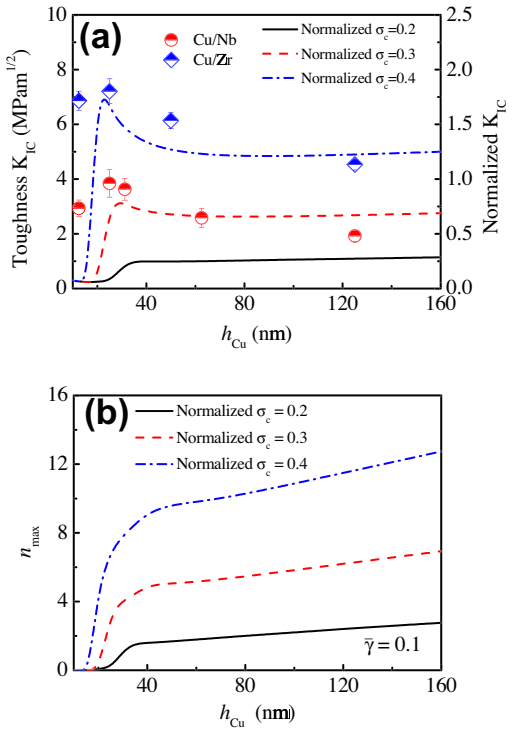

Fig. 10. (a) Dependence of K_{IC} on h_{Cu} (dots and left y-axis) for the Cu/X NMFs. Calculated normalized K_{IC} (lines and right y-axis) are also included for comparison. (b) Model predicted n_{max} at different normalized cohesive strengths ($\bar{\sigma}_c$) as a function of h_{Cu}.

In contrast to the monotonic increase in yield strength (Fig. 4), the ductility ε_C of the Cu/X NMFs reduces monotonically with increasing η (Fig. 6). Combining Eqs. (8) and (9), the toughness of Cu/X NMFs can be obtained as a function of η, which exhibited the same pattern as that of ductility. This is consistent with the general understanding that increasing the strength of a material leads to a decrease in the fracture toughness. It is the plastic work done at the crack tip during crack propagation that leads to high toughness. The amount of work done at the tip is decreased as high flow stresses impede dislocation generation and motion. In general, if the layer thickness ahead of the crack tip is smaller than the plastic zone produced on loading, there will be an alteration of the size and shape of the plastic zone, a redistribution of stresses ahead of the crack, and an effect on fracture toughness, which can be either positive or negative [1]. Here, the increase in η means a decrease in h_{Cu} and hence plays a negative role in improving the toughness.

Interestingly, a scaling relationship is revealed for both the two λ when the toughness is depicted with respect to

the yield strength, as shown in Fig. 11. This indicates that, under the constant modulation period or the same number of interfaces, the toughness of NMFs is inversely proportional to the yield strength. For example, the Cu/Nb NMFs with $\lambda = 25$ nm have a scaling slope of -8.4×10^{-3} m$^{-1/2}$, a factor of 2 higher compared with that with $\lambda = 50$ nm (about -3.7×10^{-3} m$^{-1/2}$). As mentioned above, the residual stress in the Cu/X NMFs is insensitive to both the λ and η, and the NMFs with $\lambda = 25$ and 50 nm have similar residual stresses. This indicates that the present experimental results are not predominantly related to the residual stress. Because the NMFs with $\lambda = 25$ nm contain twice as many interfaces as those with $\lambda = 50$ nm, the reason responsible for the sharper scaling slope in the former is that the dislocation movement is strongly suppressed by the increased number of interfaces. In other words, increasing the yield strength by the same level will cause a greater reduction in the fracture toughness for NMFs with thinner λ. This indicates that strengthening via interface constraint will sacrifice deformability significantly, because the movement of dislocations will be strongly suppressed by the increased number of interfaces. Once the modulation period or the microstructural feature is changed, different scaling lines will be observed. The scaling relationship between fracture toughness and yield strength revealed here could be useful when considering the optimization of a multilayer microstructure for the optimum combination of strength and fracture resistance, especially in connection with the prediction of strength by using dislocation models.

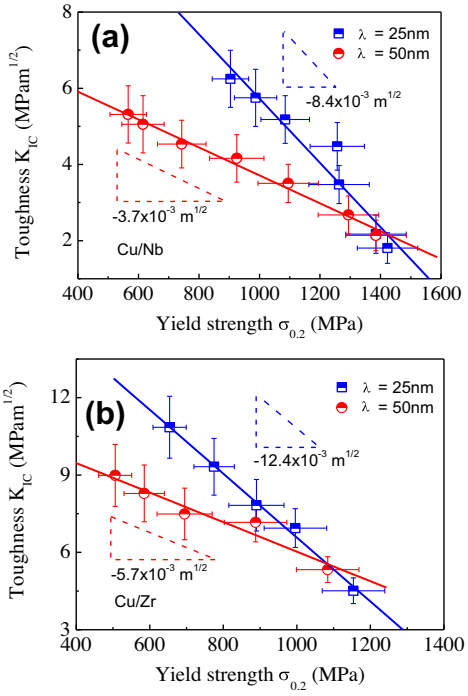

Fig. 11. Scaling relationship between toughness K_{IC} and yield strength $\sigma_{0.2}$ in (a) the Cu/Nb and (b) the Cu/Zr NMFs with $\lambda = 25$ and 50 nm, respectively.

Finally, it is necessary to address the influence of local amorphous regions on the mechanical properties in Cu/Zr NMFs. Wang et al. [18] prepared crystalline/amorphous Cu/CuZr nanolaminates and found that the continuous CuZr amorphous layers 5–10 nm thick might offer benefits in engineering the tensile plasticity of nanocrystalline metal films. On the one hand, shear banding instability is absent and so no longer affects the 5–10 nm thick nanolaminate glassy layers during tensile deformation. On the other hand, the thin amorphous layers can also act as high-capacity sinks for dislocations, enabling absorption of free volume and free energy transported by dislocations. Similarly in crystalline/amorphous Zr/CuZr multilayers, it was found that the arresting and blocking effect of the thick Zr nanocrystalline layer on incoming shear band could result in ductile plastic deformation of the thin ZrCu metallic glass layer to a high strain level of over 50% [34,39]. These results indicate that shear band formation in the very thin amorphous region could be suppressed by the thick nanocrystalline layers [18,39,40]. It is thus reasonable to believe that the 1–2 nm thick local amorphous regions will have few adverse effects on the plastic deformability of the present Cu/Zr NMFs. The benefit contributions of the local amorphous regions to mechanical properties will also be very limited, because the amorphous regions are not continuous and are very small in size. However, further work is still needed for a comprehensive understanding of the effects of local amorphous regions.

5. Conclusions

Systematic investigations of the deformation and fracture behavior of Cu/X (X = Nb, Zr) NMFs with wide ranges of λ and η have provided deep insights into the length-scale effect and constraining effect of the ductile layer on the brittle layer in terms of the mechanisms of deformability and fracture. The main findings can be summarized as follows:

(1) The yield strength of Cu/X NMFs is significantly length-scale dependent; the yield strengths were quantitatively estimated by using the CLS model when $h_{Cu} > 15$ nm and by using the ROM when $h_{Cu} < 15$ nm, considering the strongly suppressed dislocation activities by interfaces and the embrittlement of thin Cu layers, respectively.

(2) In Cu/X NMFs with $\eta = 1$, peaks are observed for both tensile ductility and fracture toughness. This unusual behavior is explained, and quantitatively assessed using a micromechanical model, by considering the competing thickness effects on the size of the microcracks initiated in the brittle X layers and on the role of the ductile Cu layer in blocking crack propagation.

(3) At a constant λ, Cu/X NMFs exhibit toughness that scales linearly with yield strength, which varies with η. The NMFs with different λ have their own scaling

relationship. The scaling slope for $\lambda = 25$ nm is much sharper than that for $\lambda = 50$ nm, indicating that a stronger interface constraint causes a greater reduction in toughness.

(4) The transition in fracture mode from opening-mode to shear-mode is generally observed in the two Cu/X NMFs and is found to be dependent on both λ and η. The fracture mode in NMFs is revealed to be controlled by the constraining effect of the ductile layer on the brittle layer rather than the transition of the deformation mechanism, which is also quantitatively assessed by using a micromechanical model.

The present experimental results and theoretical analyses provide further understanding of the plastic deformation and fracture behavior of Cu/X NMFs, and should make it possible to artificially control the constituent phases or geometrical configurations in NMFs to achieve the best combination of strength and fracture resistance.

Acknowledgements

This work was supported by the 973 Program of China (Grant No. 2010CB631003), the 111 Project of China (B06025) and the National Natural Science Foundation of China (50971097). G.L. is grateful for support from the Fundamental Research Funds for the Central Universities; G.J.Z. is grateful for support from the Program for New Century Excellent Talents in University (Grant No. NCET-10-0876); and J.Y.Z. is grateful for financial support from the China Scholarship Council (CSC).

References

[1] Was GS, Foecke T. Thin Solid Films 1996;286:1.
[2] Banerjee R, Zhang XD, Dregia SA, Fraser HL. Acta Mater 1999;47:1153.
[3] Han SM, Phillips MA, Nix WD. Acta Mater 2009;57:4473.
[4] Demkowicz MJ, Hoagland RG, Hirth JP. Phys Rev Lett 2008;100:136102.
[5] Mara NA, Bhattacharyya D, Hoagland RG, Misra A. Scripta Mater 2008;58:874.
[6] Bakonyi I, Péter L. Prog Mater Sci 2010;55:107.
[7] Misra A, Kung H. Adv Eng Mater 2001;3:217.
[8] Misra A, Hirth JP, Hoagland RG. Acta Mater 2005;53:4817.
[9] Fu EG, Li N, Misra A, Hoagland RG, Wang H, Zhang X. Mater Sci Eng A 2008;493:283.
[10] McKeown J, Misra A, Kung H, Hoagland RG, Nastasi M. Scripta Mater 2002;46:593.
[11] Liu Y, Bufford D, Wang H, Sun C, Zhang X. Acta Mater 2011;59:1924.
[12] Anderson PM, Li C. Nanostruct Mater 1995;5:349.
[13] Embury JD, Hirth JP. Acta Metall Mater 1994;42:2051.
[14] Phillips MA, Clemens BM, Nix WD. Acta Mater 2003;51:3157.
[15] Koehler JS. Phys Rev B 1970;2:547.
[16] Rao SI, Hazzledine PM. Philos Mag A 2000;80:2011.
[17] Huang H, Spaepen F. Acta Mater 2000;48:3261.
[18] Wang YM, Li J, Hamza AV, Barbee Jr TW. Proc Natl Acad Sci USA 2007;104:11155.
[19] Mara NA, Bhattacharyya D, Hirth JP, Dickerson P, Misra A. Appl Phys Lett 2010;97:021909.
[20] Mara NA, Bhattacharyya D, Dickerson P, Hoagland RG, Misra A. Appl Phys Lett 2008;92:231901.
[21] Bhattacharyya D, Mara NA, Dickerson P, Hoagland RG, Misra A. Acta Mater 2011;59:3804.
[22] Misra A, Kung H, Hammon D, Hoagland RG, Nastasi M. Int J Damage Mech 2003;12:365.
[23] Misra A, Hoagland RG. J Mater Sci 2007;42:1765.
[24] Zhu XF, Li YP, Zhang GP, Tan J, Liu Y. Appl Phys Lett 2008;92:161905.
[25] Zhang JY, Zhang X, Liu G, Wang RH, Zhang GJ, Sun J. Mater Sci Eng A. doi:10.1016/j.msea.2011.06.083.
[26] Niu RM, Liu G, Wang C, Zhang G, Ding XD, Sun J. Appl Phys Lett 2007;90:161907.
[27] Kwon KW, Lee HJ, Ryu C, Sinclair R. Acta Mater 1999;47:3965.
[28] Lai WS, Yang MJ. Appl Phys Lett 2007;90:181917.
[29] Clemens BM, Nix WD, Ramaswamy V. J Appl Phys 2000;87:2816.
[30] Zhang JY, Liu G, Wang RH, Li J, Sun J, Ma E. Phys Rev B 2010;81:172104.
[31] Zhu T, Li J. Prog Mater Sci 2010;55:710.
[32] Chen MW, Ma E, Hemker KJ, Sheng HW, Wang YM, Cheng XM. Science 2003;300:1275.
[33] Zhu XY, Luo JT, Zeng F, Pan F. Thin Solid Films. doi:10.1016/j.tsf.2010.12.251.
[34] Liu MC, Huang JC, Chou JS, Lai YH, Lee CJ, Nieh TG. Scripta Mater 2009;61:840.
[35] Hertzberg RW. Deformation and fracture mechanics of engineering materials. New York: John Wiley; 1989.
[36] Hsia KJ, Suo Z, Yang W. J Mech Phys Solids 1994;42:877.
[37] Beuth Jr JL. Int J Solids Struct 1992;29:1657.
[38] Dundurs J, Bogy DB. J Appl Mech 1969;36:650.
[39] Liu MC, Lee CJ, Lai YH, Huang JC. Thin Solid Films 2010;518:7295.
[40] Donohue A, Spaepen F, Hoagland RG, Misra A. Appl Phys Lett 2007;91:241905.